ELSEVIER Journal of Hazardous Materials 46 (1996) 253–272

JOURNAL OF HAZARDOUS MATERIALS

Numerical calculations of unsteady heavy gas dispersion

J.C.F. Pereira*, X.-Q. Chen

Instituto Superior Técnico/Technical University of Lisbon, Mechanical Engineering Department, 1096 Lisbon Codex, Portugal

Received 14 June 1994; accepted 27 January 1995

Abstract

This paper concerns both near-field and far-field numerical predictions of liquefied gas releases in atmospheric environment. The near-field prediction was related to sudden depressurization of liquefied propane into atmospheric environment. Three phases of propane vapor, propane droplets, and entrained air were considered. Simplification was made that air and vapor have the same velocity and temperature but different volume fractions so that an air–vapor mixture phase could be assumed, and was treated using an Eulerian formulation. The droplet phase was handled using a Lagrangian formulation by which droplet trajectories were computed. A thin-skin evaporation model was used to account for droplet evaporation for the near-field prediction. Present numerical results for the near-field modelling were compared with those obtained with a twin-fluid Eulerian–Eulerian model. The far-field prediction was associated with heavy gas dispersion of Burro 8 LNG field test in a flat terrain. The conventional κ–ε eddy viscosity–diffusivity model was modified to account for the anisotropy of turbulence characterized by heavy gas dispersion close to a ground. Numerical results were presented for the Burro 8 LNG field test. Results for the far field simulation were also compared with those obtained with the commercial code DEGADIS.

Keywords: Gas dispersion, Eulerian–Lagrangian model; Evaporation; Multiphase flow

1. Introduction

As it is well-known, many industrial and domestic gases are toxic and flammable, and are stored in highly-pressurized vessels at liquefied state with ambient temperature. If there is by chance a sudden depressurization, the resulting jet will consist of the gaseous air–vapour phase and liquid droplet phase with lower saturation temperature at atmospheric pressure. The violent entraining of generated vapor and ambient air tends to form a large flammable mist cloud, thus posing a great threat. The

* Corresponding author.

SSDI 0304-3894(95)00077-1

objective of this work is to numerically predict the jet flow evolution in the immediate vicinity after flashing occurrence for a propane reservoir and heavy gas dispersion from a spill source in order to provide environmental researchers with sufficient and accurate data for further investigation of later ensuing environmental problems.

The test case for this study is based on the one which has been investigated by Vandroux–Koenig et al. [1] using a twin-fluid Eulerian–Eulerian model. The present calculations are based on an Eulerian–Lagrangian hybrid model. Due to a big difference between the vessel pressure and the ambient pressure, sudden depressurization tends to cause violent entrainment between the generated vapour and the ambient air; therefore, it is assumed that a homogeneous state between the air and vapour is reached instantaneously so that these two phases could form an air–vapour mixture having the single velocity and temperature distribution. This is equivalent to saying that the air and vapour phases will have the same velocity and temperature, but have different mass fractions which are to be solved from their own governing equations and used to determine the mixture phase properties such as the voidage, density, thermal conductivity, specific heat, etc. The droplets formed after flashing are to be tracked along their trajectories based on their Lagrangian equations of motion. This treatment is an intuitive way to discriminate all droplet sizes. In Lagrangian calculations, it is assumed that droplet number flow rates are kept unchanged along their trajectories, while their diameters will be changed due to evaporation or condensation. With these simplifications and assumptions, the present problem to be considered will reduce to (i) Eulerian modelling of the mixture phase which is composed of the ambient air and propane vapour having the same velocity and temperature but different volume fractions; (ii) Lagrangian modelling of the droplet phase which is composed of various droplet-size groups having their own initial properties, i.e., the velocity, temperature, diameter, etc.

Natural gas (NG) is also often stored in the liquefied state. If there occurs an accident, NG will be released to the surrounding environment. Due to the low boiling temperature of liquefied NG, the released liquefied NG (LNG) will quickly evaporate and mix with the surrounding air to create a time-dependent, nonuniform air–NG mixture, which is flammable and hazardous. Therefore, it is often required to predict the distribution of NG concentration following the accidental spill. To predict the NG concentration, a commercial computer code DEGADIS is available. However, the DEGADIS model only predicts ensemble average gas concentrations, as pointed out by Havens [2].

At present, available high-speed computers make it possible to simulate the evolution of LNG spill over the surrounding environment using a time-dependent, three-dimensional flow model. Therefore, the objective of this work is to develop a time-dependent, three-dimensional numerical model capable of predicting the evolution of gas dispersion posterior to the spill. The numerical model is validated against the Burro 8 field test. However, comparisons are only made between present results and those obtained with the commercial DEGADIS code. The previous study by Betts and Haroutunian [3] was based on the finite-element method, where the strong anisotropy of turbulent diffusion peculiar to heavy gas dispersion close to the ground was accounted for, and it was found that the model could capture the main

characteristics of Burro 8 field test. Hence, their anisotropically turbulent dispersion model was also adopted in the present work.

2. Governing equations for the near-field modelling

The k–ε eddy viscosity–diffusivity model is used for the turbulence closure. The general form of equations for two-dimensional multiphase flows in either cartesian or cylindrical coordinate can be written as:

$$\frac{\partial \rho \alpha y^m \phi}{\partial t} + \frac{\partial \rho \alpha y^m U_j \phi}{\partial x_j} = \frac{\partial}{\partial x_j}\left(\alpha y^m \Gamma \frac{\partial \phi}{\partial x_j}\right) + y^m S_\phi + S_\phi^p, \tag{1}$$

where ϕ is any one of the dependent variables: U, V, k, ε, and H; α stands for any one of the voidages: α_a, α_v, α_m; Γ is the diffusion coefficient; S_ϕ and S_ϕ^p represent the source terms arising from the gas phase itself and the external droplet phase, respectively. The superscript 'm' in Eq. (1) is used to identify flow configuration with $m \equiv 0$ for planar flows and $m \equiv 1$ for axisymmetric flows. Detailed expressions for these variables are tabulated in Table 1. The global volume conservation yields

$$\alpha_a + \alpha_v + \alpha_p = 1, \tag{2}$$

Table 1
Coefficients of Eq. (1)

ϕ	α	Γ	ρ	S_ϕ	S_ϕ^p
1	α_a	0	ρ_a	0	0
1	α_v	0	ρ_v	0	$\sum_i \dot{n}_i (m_{p,\text{in}} - m_{p,\text{out}})$
U	α_m	μ_m	ρ_m	$-\alpha_m \frac{\partial P}{\partial x} + \frac{\partial}{\partial x}\left(\alpha_m \mu_m \frac{\partial U}{\partial x}\right) + \frac{1}{y^m}\frac{\partial}{\partial y}\left(\alpha_m \mu_m y^m \frac{\partial V}{\partial x}\right)$	$\sum_i \dot{n}_i (m_{p,\text{in}} u_{p,\text{in}} - m_{p,\text{out}} u_{p,\text{out}})$
V	α_m	μ_m	ρ_m	$-\alpha_m \frac{\partial P}{\partial y} + \frac{\partial}{\partial x}\left(\alpha_m \mu_m \frac{\partial U}{\partial y}\right) + \frac{1}{y^m}\frac{\partial}{\partial y}\left(\alpha_m \mu_m y^m \frac{\partial V}{\partial y}\right) - \frac{2m\mu_m \alpha_m V}{y^{3m}}$	$\sum_i \dot{n}_i (m_{p,\text{in}} v_{p,\text{in}} - m_{p,\text{out}} v_{p,\text{out}})$
k	α_m	μ_m/σ_k	ρ_m	$\alpha_m \rho_m (G - \varepsilon)/y^m$	0
ε	α_m	μ_m/σ_ε	ρ_m	$\alpha_m \rho_m \frac{\varepsilon}{y^m k}(C_{\varepsilon 1} G - C_{\varepsilon 2}\varepsilon)$	0
H	α_m	μ_m/σ_h	ρ_m	0	$\sum_i \dot{n}_i (m_{p,\text{in}} h_{p,\text{in}} - m_{p,\text{out}} h_{p,\text{out}})$

$$G = \frac{\mu_m}{\rho_m}\left\{2\left[\left(\frac{\partial U}{\partial x}\right)^2 + \left(\frac{\partial V}{\partial y}\right)^2\right] + m\left(\frac{V}{y_m}\right)^2 + \left(\frac{\partial U}{\partial y} + \frac{\partial V}{\partial x}\right)^2\right\}, \quad \mu_m = \rho_m C\mu \frac{k^2}{\varepsilon}$$

$C_\mu = 0.09, C_{\varepsilon 1} = 1.44, C_{\varepsilon 2} = 1.92, \sigma_k = 1.0, \sigma_\varepsilon = 1.3, \sigma_h = 0.9$

where α_p denotes the droplet voidage. Based on its definition, the mixture voidage α_m is the summation of α_a and α_v; therefore, it follows

$$\alpha_a + \alpha_v = \alpha_m = 1 - \alpha_p. \tag{3}$$

The droplet voidage, α_p, is directly calculated in the Lagrangian tracking procedure.

In the Lagrangian calculations, the two-way coupling between the droplet- and gas-phases can be easily performed by computing what is lost or gained in terms of mass, momentum, and energy in the Eulerian cell crossed. Generally speaking, forces acting on a droplet include a variety of terms, i.e., the terms of aerodynamic drag, Magnus, Basset, Saffman, thrust, etc. In practice, it is often accurate enough to account for only the drag force when the ratio of the gas to droplet densities is very small. This simplification is verified theoretically by Faeth [4], and he came to the conclusion by estimating the order of magnitude of these forces. Based on this simplification, the equation of motion for each size of droplets can be written as

$$\frac{du_{pi}}{dt} = \frac{\tilde{u}_i - u_{pi}}{\tau_p} + F_{pi}, \tag{4}$$

where F_{pi} is an external force acting on a droplet, i.e., the centrifugal force for axisymmetric flows. In Lagrangian stochastic models, the instantaneous gas velocity in Eq. (4) is obtained by summing the mean value over the fluctuating value; that is,

$$\tilde{u}_i = U_i + u_i'. \tag{5}$$

The calculation of the gas-phase fluctuating velocity depends on the stochastic model selected. In Lagrangian deterministic models, however, only the mean velocity is used. For the present dense multiphase propane flashing flow, only the Lagrangian deterministic model was employed. τ_p is the droplet relaxation time, defined by

$$\tau_p = \frac{\rho_p D_p^2}{18\mu f_p}, \qquad f_p = 1 + 0.15 Re_p^{0.687}, \tag{6}$$

where the relative Reynolds number is given by

$$Re_p = \frac{\rho D_p \sqrt{(u_i - u_{pi})^2}}{\mu}. \tag{7}$$

The droplet trajectories for a two-dimensional flow are obtained by integrating their velocities as follows:

$$\frac{dx_{pi}}{dt} = u_{pi}. \tag{8}$$

The droplet voidage can be computed by summing over all the droplet volume within the Eulerian cell during Lagrangian tracking. At present droplet evaporation is accounted for using a thin-skin model, based on the heat balance that the heat transferred from the gas-phase to the droplet-phase contributes completely to droplet evaporation. Therefore, the heat balance equation can be written as

$$\dot{m}L = \pi Nu\, k_c D_p (T - T_p), \tag{9}$$

where $\dot{m}$ is the mass evaporation rate, L the latent heat of vaporization, Nu the Nusselt number, k_c the thermal conductivity of the air–vapour mixture. The droplet surface temperature is assumed to be its saturation temperature at atmospheric pressure. Using Eq. (9), we can obtain

$$\frac{dD_p}{dt} = -\frac{2Nu\,k_c(T - T_p)}{\rho_p D_p}. \tag{10}$$

The Nusselt number, Nu, is computed by using

$$Nu = 2 + 0.6Re_p^{1/2}Pr^{1/3}. \tag{11}$$

3. Governing equations for the far-field modelling

To predict heavy gas dispersion in the far field, the buoyant generation has to be considered, and it is recommendable to account for the anisotropy of turbulent diffusion peculiar to heavy gas dispersion close to the ground. A three-dimensional computation was performed for the present far-field modelling. The governing equations are slightly different from those listed in Table 1. For completeness and easy description, they are still written here. The Reynolds' time averaging equations for mass, momentum, energy and concentration can be written tensorially as follows:

$$\frac{\partial \rho}{\partial t} + \frac{\partial \rho U_j}{\partial x_j} = 0 \tag{12}$$

$$\frac{\partial \rho U_i}{\partial t} + \frac{\partial \rho U_i U_j}{\partial x_j} = -\frac{\partial P}{\partial x_i} + \frac{\partial}{\partial x_j}\left(\mu \frac{\partial U_i}{\partial x_j} - \overline{\rho u_i' u_j'}\right) + (\rho - \rho_a) g_i, \tag{13}$$

$$\frac{\partial \rho H}{\partial t} + \frac{\partial \rho U_j H}{\partial x_j} = \frac{\partial}{\partial x_j}\left(\frac{\mu}{Pr}\frac{\partial H}{\partial x_j} - \overline{\rho u_j' h'}\right), \tag{14}$$

$$\frac{\partial \rho C}{\partial t} + \frac{\partial \rho U_j C}{\partial x_j} = \frac{\partial}{\partial x_j}\left(\frac{\mu}{Sc}\frac{\partial C}{\partial x_j} - \overline{\rho u_j' c'}\right), \tag{15}$$

where the overbars stand for time averaging and $Pr = Sc = 0.7$. The enthalpy is computed by

$$H = C_p T \qquad C_p = C_{pa}(1 - C) + C_{pv}C. \tag{16}$$

The k–ε eddy viscosity–diffusivity model is used for turbulence closure. The additional transport equations for turbulence kinetic energy and its dissipation rate are given by

$$\frac{\partial \rho k}{\partial t} + \frac{\partial \rho U_j k}{\partial x_j} = \frac{\partial}{\partial x_i}\left[\left(\mu \delta_{ij} + \frac{\mu_{ij}}{\sigma_k}\right)\frac{\partial k}{\partial x_j}\right] + G - \rho\varepsilon + B, \tag{17}$$

$$\frac{\partial \rho \varepsilon}{\partial t} + \frac{\partial \rho U_j \varepsilon}{\partial x_j} = \frac{\partial}{\partial x_i}\left[\left(\mu \delta_{ij} + \frac{\mu_{ij}}{\sigma \varepsilon}\right)\frac{\partial \varepsilon}{\partial x_j}\right] + C_{\varepsilon 1}\frac{\varepsilon}{k}G + C_{\varepsilon 1}(1 - C_{\varepsilon 3})\frac{\varepsilon}{k}B - C_{\varepsilon 2}\rho\frac{\varepsilon^2}{k}, \tag{18}$$

with the turbulent generation G and buoyant term B defined by

$$G = -\overline{\rho u_i' u_j'}\frac{\partial U_i}{\partial x_j}, \qquad B = -\overline{\rho' u_i'}\, g_i. \tag{19}$$

All the standard coefficients are used for the k–ε turbulence closure; see Table 1. However, $C_{\varepsilon 3}$ is modified following the suggestion of Betts and Haroutunian [3]. The coefficient $C_{\varepsilon 3}$ is given by

$$C_{\varepsilon 3} = \begin{cases} -0.8 & B \geqslant 0 \\ 2.15 & B < 0 \end{cases}. \tag{20}$$

The fluctuating correlations are modeled as follows:

$$-\overline{\rho u_i' h'} = \frac{\mu_{ij}}{\sigma_t}\frac{\partial H}{\partial x_j}, \qquad -\overline{\rho u_i' c'} = \frac{\mu_{ij}}{\sigma_t}\frac{\partial C}{\partial x_j}, \tag{21}$$

$$-\overline{\rho' u_i'} = \frac{\mu_{ij}}{\rho\sigma_t}\frac{\partial \rho}{\partial x_j}, \qquad -\overline{\rho u_i' u_j'} = \kappa_{lm}\delta_{li}\left(\frac{\partial U_m}{\partial x_l} + \frac{\partial U_l}{\partial x_m}\right) - \frac{2}{3}\rho k\delta_{ij}, \tag{22}$$

where δ_{ij} is the Kronecker delta function. The turbulent eddy viscosity μ_{ij} has taken into account the anisotropy of turbulence associated with the heavy gas dispersion [3]:

$$\mu_{ij} = \begin{Bmatrix} \overline{v'^2}/\overline{w'^2}\,\mu_t & 0 & 0 \\ 0 & \mu_t & 0 \\ 0 & 0 & \mu_t \end{Bmatrix}, \qquad \mu_t = \rho C_\mu \frac{k^2}{\varepsilon}. \tag{23}$$

The anisotropic turbulent diffusivity, κ_{lm}, in Eq. (22) is given by

$$\kappa_{lm} = \begin{Bmatrix} \mu_t & \overline{v'^2}/\overline{w'^2}\,\mu_t & \mu_t \\ \overline{v'^2}/\overline{w'^2}\,\mu_t & \mu_t & \mu_t \\ \mu_t & \mu_t & \mu_t \end{Bmatrix}. \tag{24}$$

The definition of κ_{lm} in Eq. (24) follows the suggestion of Betts and Haroutunian [3], which has accounted for the strong anisotropy of turbulent diffusion encountered in stratified flows close to the ground boundary. The ratio of the local cross-wind velocity variance $\overline{v'^2}$ to the local vertical velocity variance $\overline{w'^2}$ is used to account for the anisotropy of turbulent diffusion due to heavy gas dispersion. The two velocity variances are obtained, due to Gibson and Launder [5] by

$$\frac{\overline{w'^2}}{k} = \frac{2}{5.4 + 3f_w}\left[1.4 - 0.36f_w - (1.4 + 0.36f_w)\left(\frac{-B}{G+B}\right)\right] \tag{25a}$$

$$\frac{\overline{v'^2}}{k} = 0.518 + \left(0.066 + \frac{\overline{w'^2}}{k}\right) f_w + (0.037 + 0.066 f_w)\left(\frac{-B}{G+B}\right) \tag{25b}$$

from which the ratio of $\overline{v'^2}$ to $\overline{w'^2}$ can be determined straightforwardly. The near-wall function, f_w, is given by

$$f_w = \frac{C_\mu^{3/4} k^{3/2}}{\kappa \varepsilon z} \tag{26}$$

with κ being the von Karman constant, equal to 0.41.

In the present modified k–ε model, the turbulent Prandtl/Schmidt number σ_t is assumed to be a function of the local nondimensional buoyancy parameter [5], instead of being constant which is widely adopted in many conventional k–ε models:

$$\sigma_t = \frac{\beta_1 - 0.22\beta\beta_2}{\beta_3 - (1.6\beta_4 - 0.33\beta_2)}, \tag{27}$$

where β's are defined by

$$\beta_1 = \frac{0.4 + 0.27 f_w}{1.8 + 0.75 f_w}, \qquad \beta_2 = \frac{0.5}{1.8 + 0.75 f_w}, \tag{28a}$$

$$\beta_3 = \frac{1}{3 + 0.5 f_w}, \qquad \beta_4 = \frac{2}{9 + 1.5 f_w}, \qquad \beta = \frac{k}{\overline{w'^2}} \frac{-B}{G+B}, \tag{28b}$$

by which the turbulent Prandtl/Schmidt number can be determined. Note that the mixture density of air and NG is computed by the equation of state:

$$\rho = \frac{P}{RT[C/W_v + (1-C)/W_a]} \tag{30}$$

where W_a and W_v are the molecular weights of air and NG, respectively, R the gas universal constant.

4. Initial and boundary conditions

At present, the near-field modeling was carried out for steady situations. The axial mean velocity for propane droplets and vapor was 50 m/s at the inlet. No radial velocity was present at the inlet. Two typical droplet sizes were considered, and two runs were performed using the same initial velocity distribution but different propane droplet- and vapor-voidage distributions:

(i) $\alpha_v = 0.7$, $\alpha_p = 0.3$, $\alpha_a = 0.0$, $D_{p1} = 10$ μm, $D_{p2} = 50$ μm;

(ii) $\alpha_v = 0.9$, $\alpha_p = 0.1$, $\alpha_a = 0.0$, $D_{p1} = 10$ μm, $D_{p2} = 50$ μm.

The droplet mass fractions are 2/3 and 1/3 for the small and big droplet diameters, respectively. The inlet temperature was the atmospheric temperature, equal to 293 K.

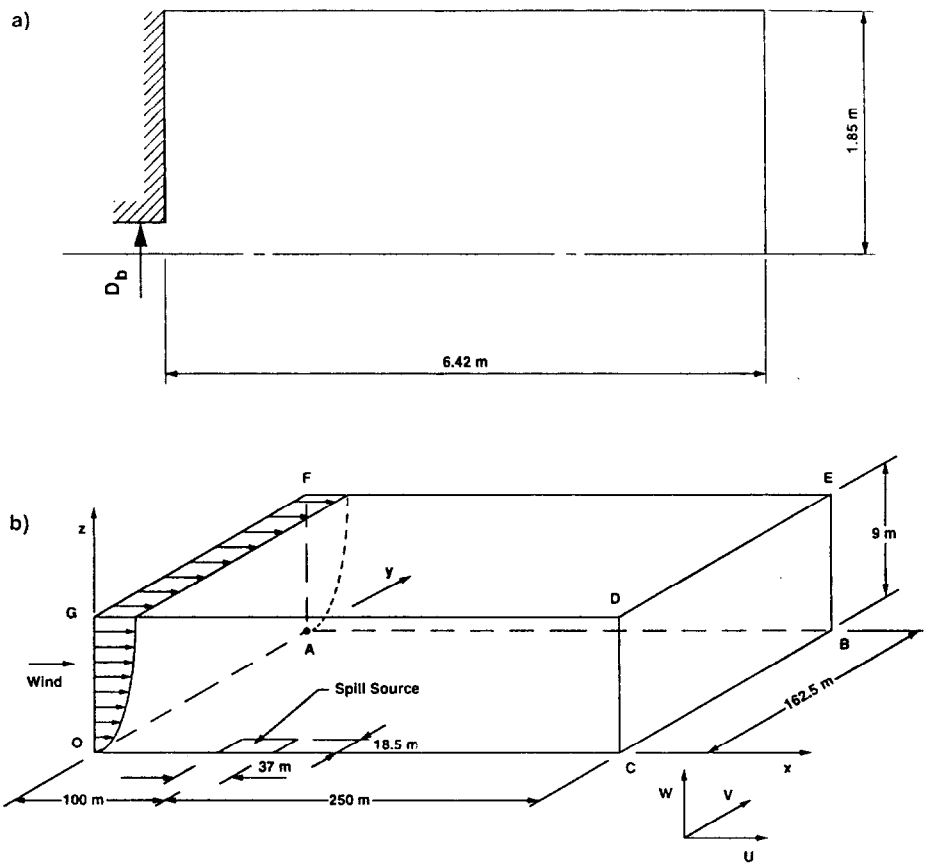

Fig. 1. Geometry of (a) near-field modeling and (b) far-field modeling.

The computational domain is shown in Fig. 1(a) for the first run. The computational domain is covered by a grid 37×18 nodes. However, a multicomputational-domain method was used for the second run, each domain covered by a grid of 37×18. Details on this method can be found elsewhere [6, 7]. For the far-field modelling, an unsteady computation was performed. To start with the unsteady calculation, it is necessary to assign an initial flowfield. The initial conditions corresponding to the atmospheric situation for the Burro 8 field test can be found in detail elsewhere [3]. The flow geometry for the three-dimensional computation is shown in Fig. 1(b). The spill source was $37 \times 18.5\ m^2$, and had a vertical release velocity of 0.064 m/s. A grid of $36 \times 32 \times 18$ was used to cover the whole computational domain.

The finite-volume method of Patankar [8] was used to discretize the differential equations. The discretized finite-difference equations were solved using the line-by-line TDMA solver. The time step for the unsteady far-field modeling was taken as 0.5 s.

5. Results and comparisons

Shown in Figs. 2(a) and (b) are, respectively, the droplet-phase and gas-phase velocity vectors for the first run. It can be seen that the radial dispersion is very small for both the gas- and droplet-phases due to the big initial axial velocity and zero radial velocity at the inlet.

The mixture-phase temperature contour is shown in Fig. 3(a). The central jet temperature is close to the saturation temperature of the propane liquid. This is because the mass loading of propane liquid at the inlet is so high that droplets can completely cool the mixture in this region. The eventual heat balance is reached that the energy extracted by the droplet from the mixture is equal to that required for the heat of vaporization. Far away from the jet center, the mixture-phase temperature is almost the same as the ambient temperature. This is very intuitive, as there are no droplets present there. Shown in Figs. 3(b) and (c) are the voidage contours for the vapor- and droplet-phases. Due to the small radial dispersion, these contours vary very steeply in the radial direction, and are concentrated near the central jet region. The vapor-phase dispersion is relatively larger than the droplet-phase.

Due to the unavailable experimental measurements, the present numerical predictions cannot be directly validated against the data. Therefore, comparisons are made here between present Eulerian–Lagrangian results with Eulerian–Eulerian results from Vandroux–Koenig [9]. The numerical predictions were obtained using the initial conditions for the second run. It should be emphasized that Vandroux–Koenig [9] used only single size of droplet diameters equal to 10 μm. Figs. 4(a)–(c) show the comparison of the mixture-phase temperatures between the present Eulerian–Lagrangian and Vandroux–Koenig's Eulerian-Eulerian calculations at (a) $X = 2.55$ m, (b) $X = 6.15$ m and (c) $X = 10.9$ m. The present Eulerian–Lagrangian model predicts a larger jet expansion, as compared to the Eulerian–Eulerian model. The reason may be due to the fact that the present results were obtained by solving the equation for the turbulent kinetic energy explicitly, whereas the results from Vandrous-Koenig [9] were obtained by incorporating implicitly the turbulent diffusion terms in the momentum equations. As a consequence, the jet expansion may be underpredicted. The discrepancy between the two model predictions is relatively small until $X = 6.15$ m. However, there exists large discrepancy far downstream at $X = 10.9$ m. The present results were obtained by using eight sequential boxes to cover a large computational domain up to 50 m, while the Eulerian–Eulerian results were obtained using only one computational domain to cover the same domain. It is expected that numerically the refined grids should improve the predictions. Figs. 5(a)–(c) show the comparison of the vapour voidages between the two calculations at the three axial stations. Compared with the present Eulerian–Lagrangian model, the underprediction of the jet expansion with the Eulerian–Eulerian model can still be observed in these figures. Much steep change of the vapor voidages away from the jet center is obvious in the predictions of Vandroux–Koenig [9]. The most probable reason for this discrepancy is due to the treatment of the turbulent diffusion and the numerical accuracy as explained before. Figs. 6(a)–(e) show the comparison of the mixture-phase axial mean velocities obtained with the present Eulerian–Lagrangian model and with

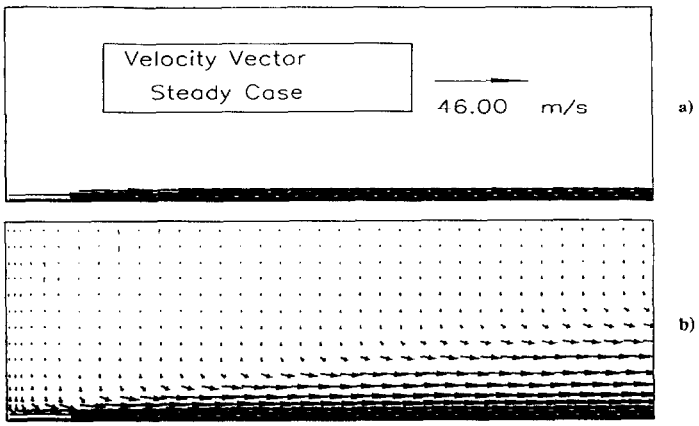

Fig. 2. Velocity vectors of (a) droplet phase and (b) mixture phase.

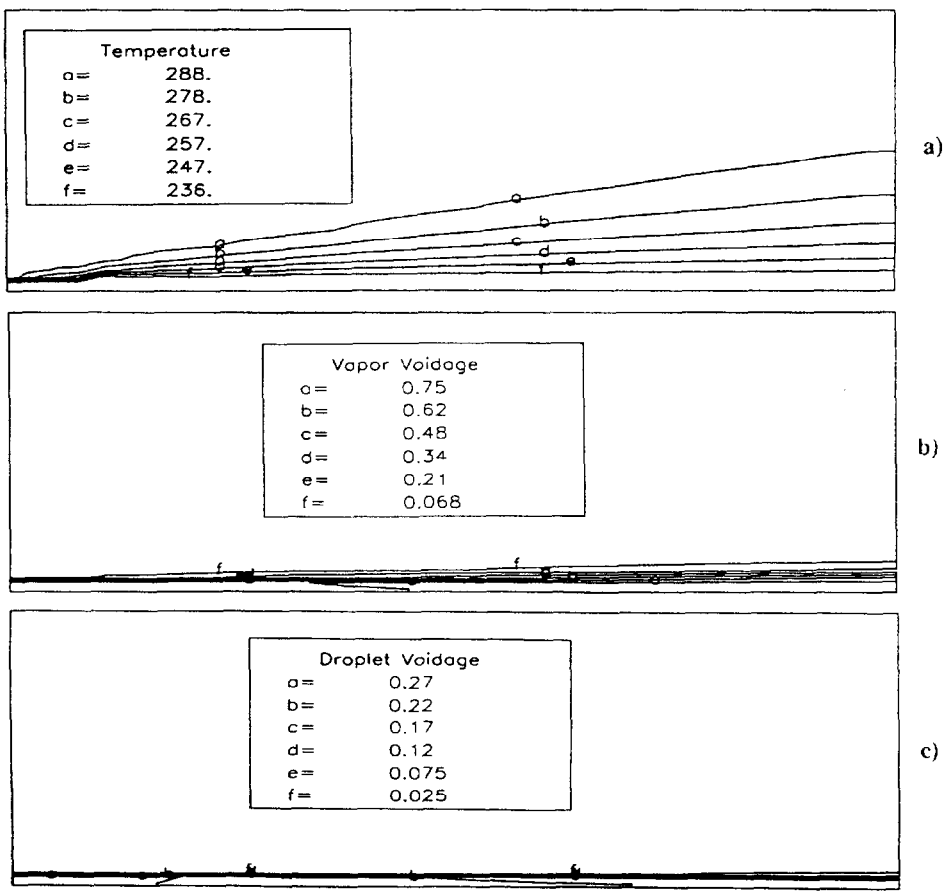

Fig. 3. Contours of (a) gas temperature, (b) vapor voidage, and (c) droplet voidage.

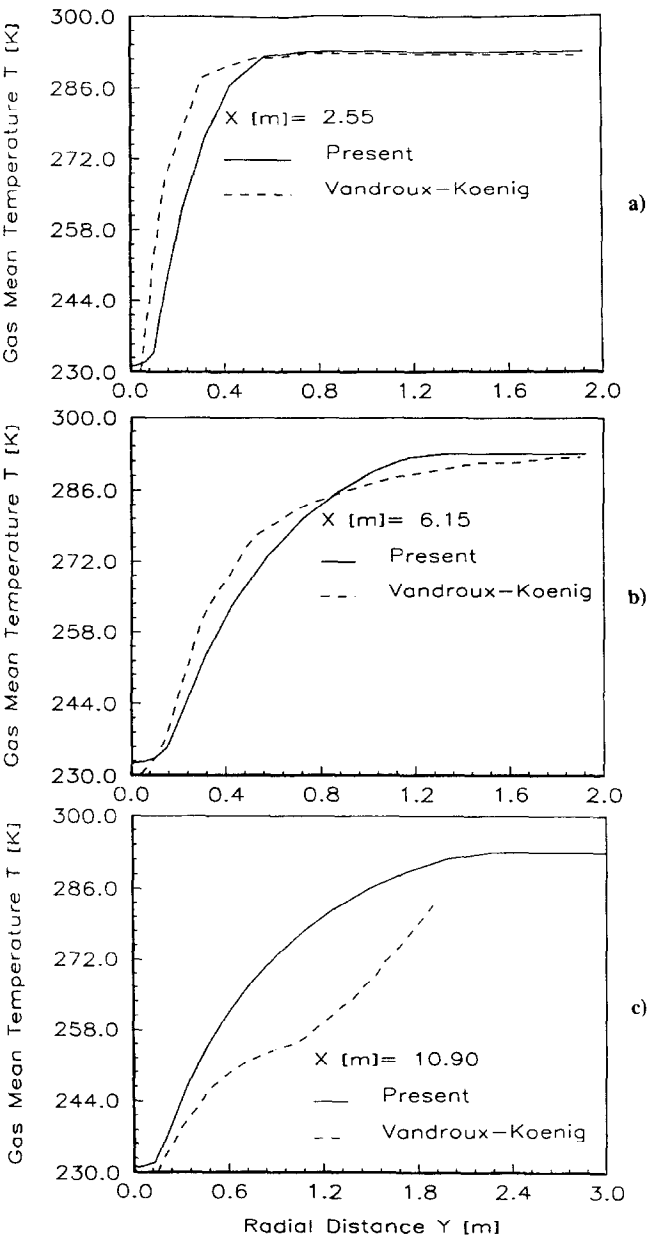

Fig. 4. Comparison of mixture-phase temperature.

the Eulerian–Eulerian model at five axial stations. It can be seen that farther downstream at $X = 15.7$ m and 27.7 m the two predictions agree reasonably well. The relatively large discrepancies are still present upstream of $X = 10.9$ m. The important reason for these discrepancies is attributed to the droplet sizes used for computations.

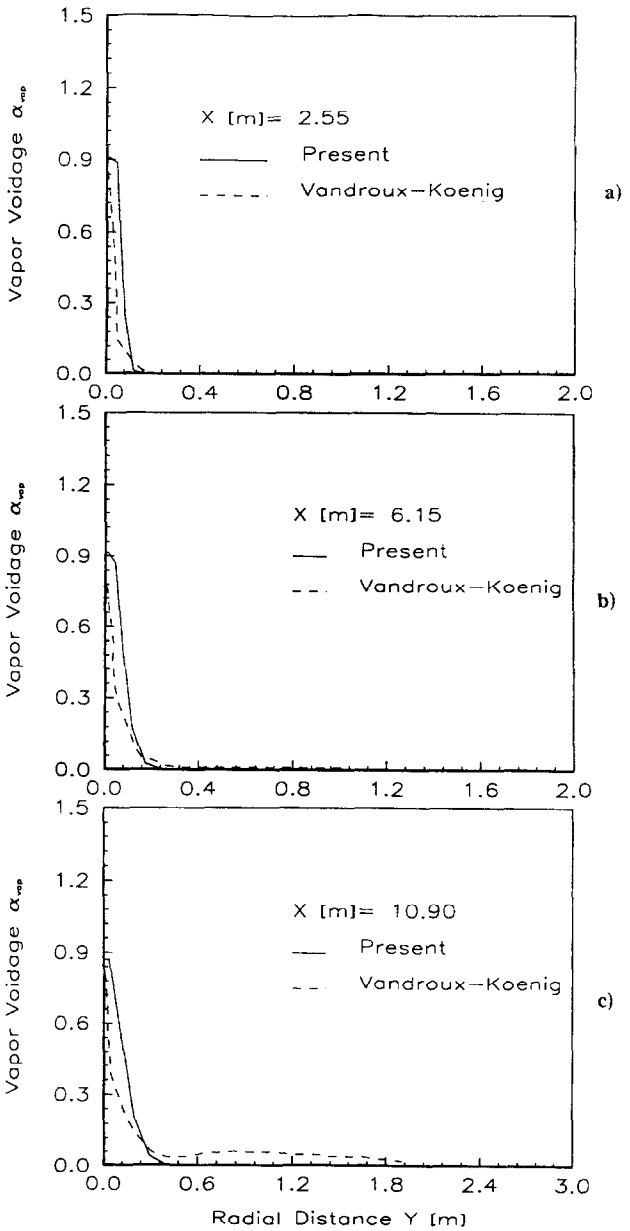

Fig. 5. Comparison of propane vapor voidage.

The present results were based on two droplet sizes whereas the Eulerian–Eulerian results were only based on single small droplets. Small droplets have less inertia than big droplets; therefore, smaller droplets are easier to lose their inertia as compared to big droplets. On the other hand, the present multiphase flow is characterized by

strong two-way coupling between the mixture phase and droplet phase owing to high mass loading at the inlet. As a result, the present axial mean velocity obtained with the presence of big droplets is overpredicted as compared to the Eulerian–Eulerian results

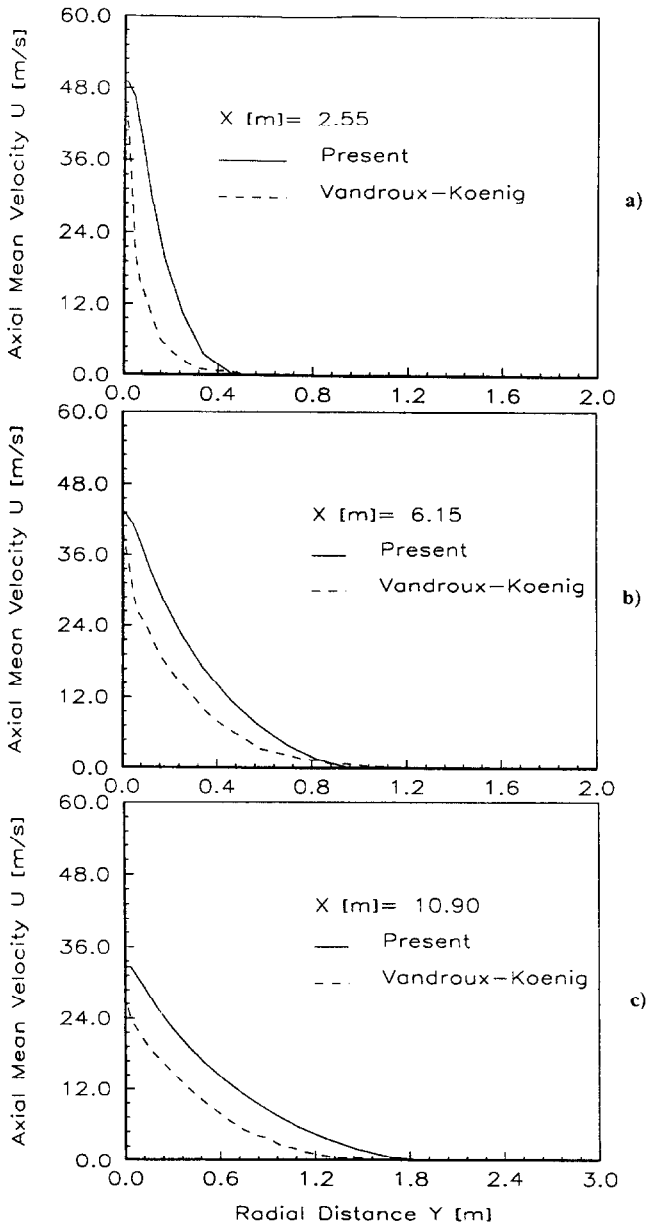

Fig. 6. Comparison of mixture-phase velocity.

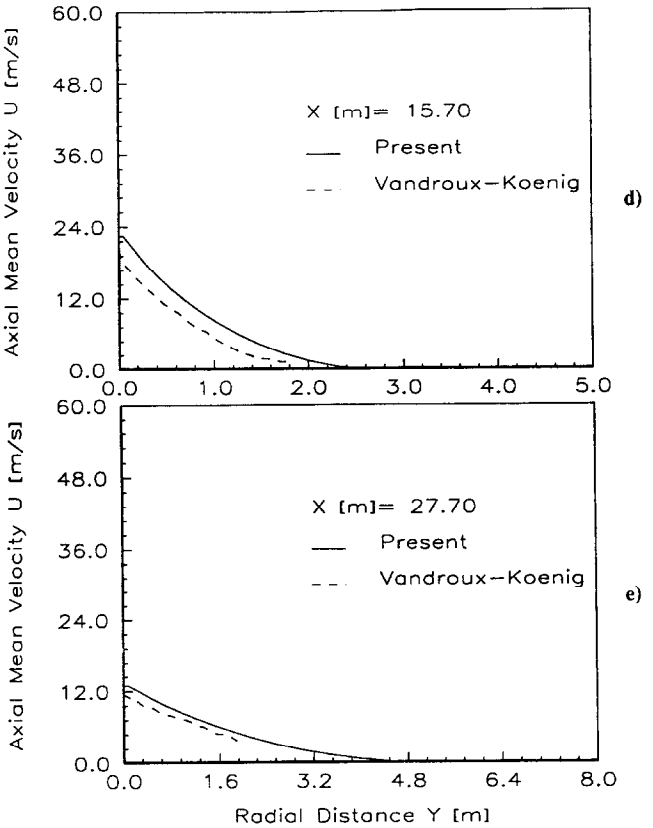

Fig. 6. Continued.

obtained with the presence of only small droplets. The results for the far-field modeling are presented as follows.

Figs. 7 and 8 show the evolution of NG concentration at $z = 0.3$ m and 0.8 m for different instants of 30 s, 50 s, 70 s, and 90 s. From these figures, it can be seen that heavy gas is convected downstream due to wind blowing effects, and that heavy gas dispersion increases as time elapses. Note that some concentration levels are not plotted in these figures further over the ground, which means that these concentration levels are not present in the horizontal plane at that height. Figs. 9(a)–(c) show the velocity vectors in a vertical plane at $y = 9.25$ m (the middle of the spill source) for different instants. The initial wind velocity profiles are distorted by the presence of released NG in the region close to the spill source. Similarly to the vapor concentration contours, the evolution of heavy gas dispersion with time can be clearly observed in these figures.

Shown in Fig. 10 are the comparisons of NG concentration at $z = 0.3$ m between the present model and the DEGADIS model. Bear it in mind that

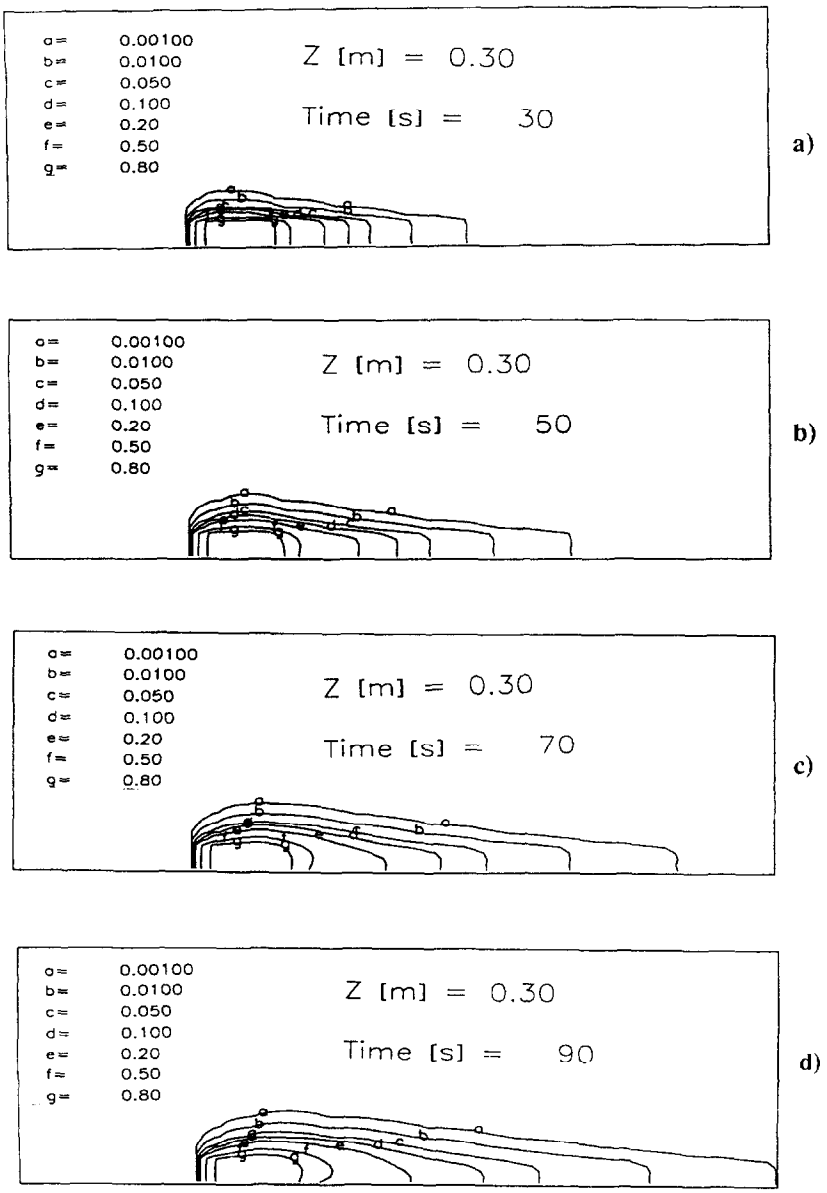

Fig. 7. Evolution of NG concentration contours at $z = 0.3$ m.

the DEGADIS model gives the mole fraction, which has to be converted into volume concentration based on the molecular weight and density for direct comparison. Fig. 10 shows that close to the ground the one-dimensional DEGADIS model can yield NG concentration predictions agreeable with the present three-dimen-

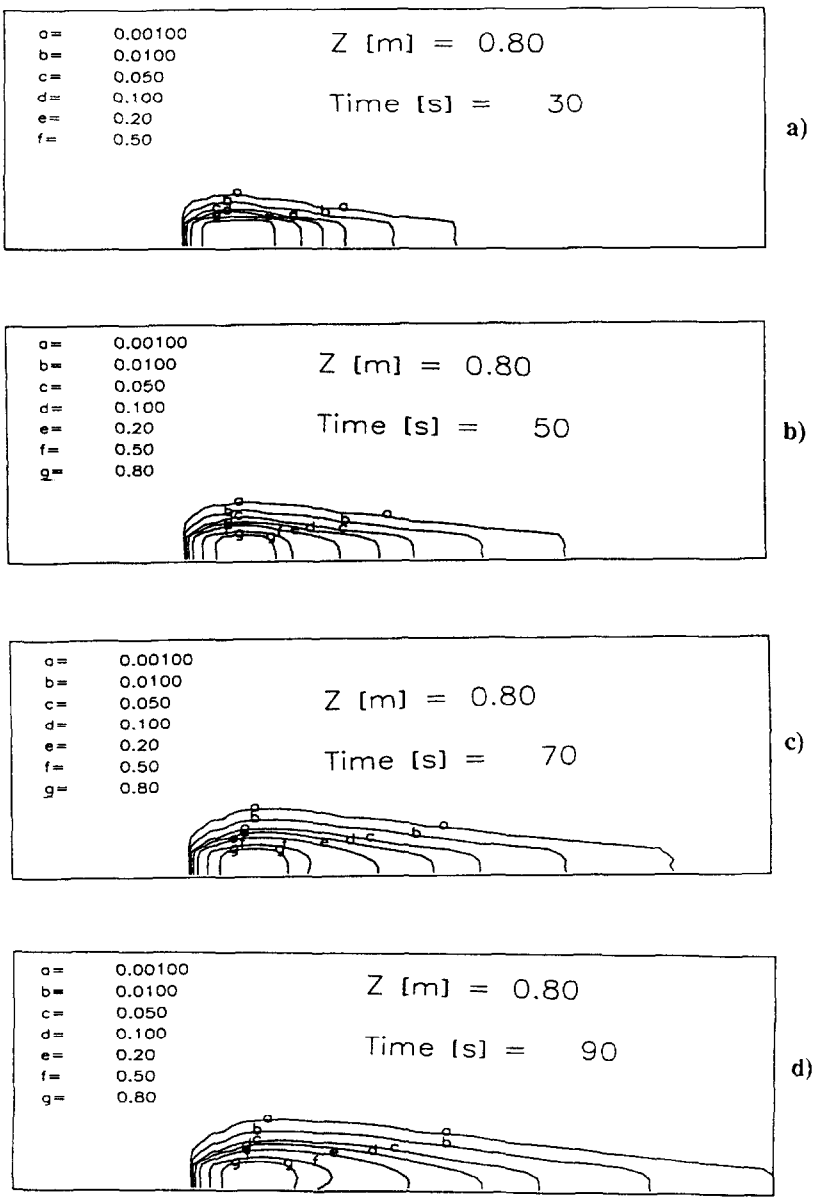

Fig. 8. Evolution of NG concentration contours at $z = 0.8$ m.

sional computations. Due to the lack of space, comparisons are not made between the two models for other heights. It can be expected that discrepancy will exist between the two models for the concentration predictions far away from the ground.

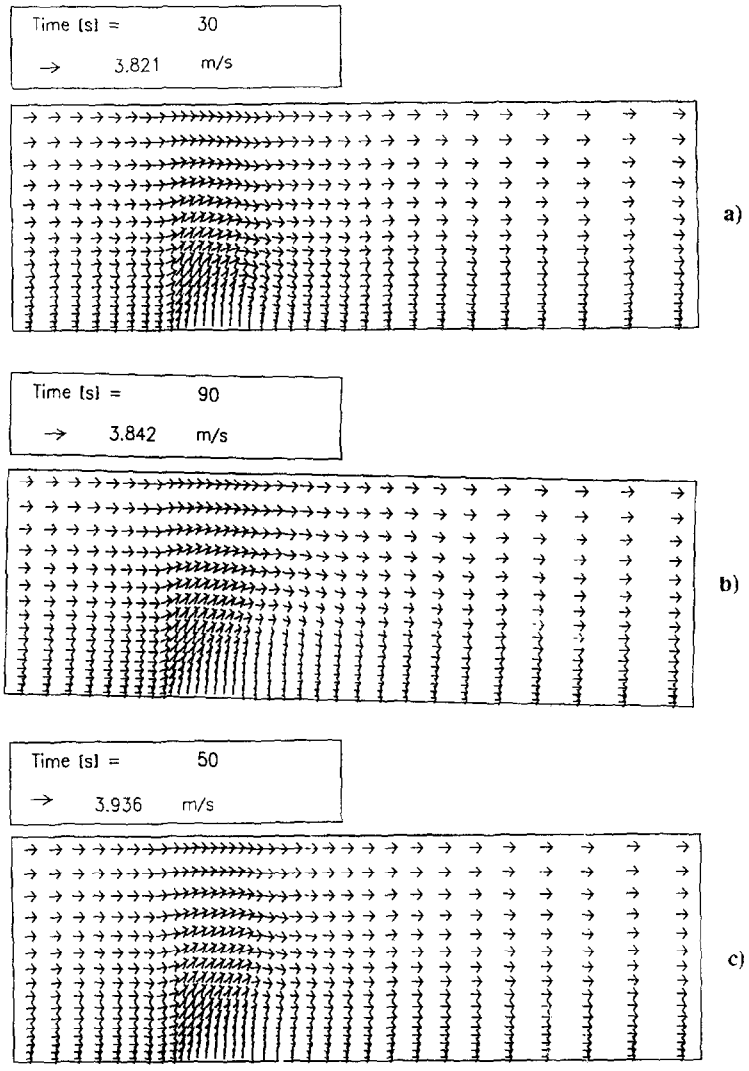

Fig. 9. Evolution of velocity vectors (U, W) at $y = 9.25$ m.

6. Concluding remarks

Numerical predictions were presented for both the near-field and far-field situations. The near-field results were compared with those obtained with the Eulerian–Eulerian model, showing the consistency between the two models. However, discrepancy was still present due to the different droplet sizes, turbulent models, etc. considered in the two models. Further validation of the present numerical model can

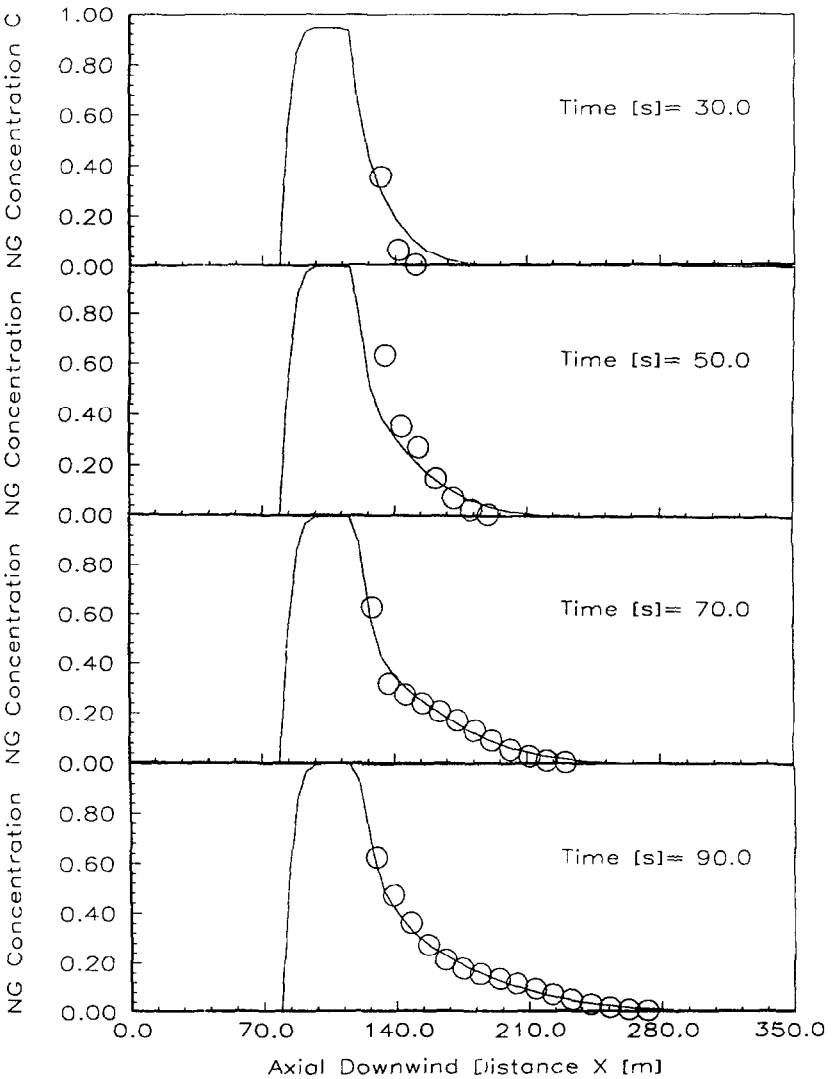

Fig. 10. Comparison of NG concentrations with DEGADIS model.

only rely on experimental measurements. The far-field predictions were obtained using a modified k–ε model which accounts for the anisotropy of turbulent diffusion peculiar to heavy gas dispersion close to the ground, and compared with those obtained with the commercial computer code DEGADIS. The NG concentration predicted by the present model was comparable with that predicted by the DEGADIS. However, the present three-dimensional model can provide more detailed flowfields than the DEGADIS model which can only predict ensemble gas dispersion.

Acknowledgements

The present work was supported by the European Communities under the contract No. STEP-CT90-0091-(SMA) entitled "Lagrangian Modeling of Multidimensional Two-Phase Flows Following an Accidental Bottom Discharge of a Liquefied Propane Tank". The results obtained with the DEGADIS model were carried out by Miss Isabel Malico,whose work is gratefully acknowleged.

Nomenclature

$\dot{n}_i$	number flow rate of droplet size i
B	buoyancy force
C	NG concentration
C_p	specific heat at constant pressure
H	mean and fluctuating enthalpies
k	turbulent kinetic energy
P	pressure
Pr	Prandtl number
Sc	Schmidt number
T	temperature
t	time
U	velocity
x	coordinate

Greek symbols

ε	dissipation rate of k
μ	dynamic viscosity
ρ	density

Subscripts

a	air
i, j	cartesian coordinates
t	turbulent
v	NG or vapor

References

[1] S. Vandroux–Koenig, G. Berthoud, D. Cordero, H. Kahn and P. Mercier, Modelling of Multiphase Jets in the Immediate Vicinity of a Containment Breach: Application to a Propane Reservoir, Note Technique STR/LML/91-21, Grenoble, France, 1991.

[2] J. Havens, J. Loss Prev. Process Ind., 5 (1992) 28.

[3] P.L. Betts and V. Haroutunian, in J.S. Puttock (Ed.), IMA Conf. Series, New Series No. 15, O.U.P., 1988, p. 349.
[4] G.M. Faeth, Prog. Energy Combust. Sci., 3 (1977) 191.
[5] M.M. Gibson and B.E. Launder, J. Fluid Mech., 86 (1978) 491.
[6] D.F.G. Durão and J.C.F. Pereira, Appl. Math. Modeling, 15 (1991) 338.
[7] X.-Q. Chen and J.C.F. Pereira, Atomization and Sprays, 2 (1992) 427.
[8] S.V. Patankar, Numerical Heat and Fluid Flow, Hemisphere Publishing House, McGraw-Hill, 1980.
[9] S. Vandroux-Koenig, Modelling of a Multiphase Jet Following a Propane Tank Ruputure, Step Report, Grenoble, April 6–7, France, 1994.